Proceedings of the ASME 2019 Conference on Smart Materials, Adaptive Structures, and Intelligent Systems Conference
SMASIS2019
September 9-11, 2019, Louisville, KY, USA

SMASIS2019-5588

INTEGRATED ROTOR PERFORMANCE IMPROVEMENT AND VIBRATION REDUCTION USING ACTIVE CAMBER MORPHING

Sumeet Kumar*, Dominik Komp, Manfred Hajek, Jürgen Rauleder
Institute of Helicopter Technology
Technical University of Munich
Munich 85748, Germany

ABSTRACT

This paper discusses open-loop and closed-loop active control investigations of a full-scale Bo 105 helicopter rotor with active camber morphing. The potential of an active camber morphing concept to reduce non-rotating vibratory hub loads and rotor power using active control was investigated. The mechanism employed was a dynamically actuated airfoil camber morphing concept known as Fish Bone Active Camber (FishBAC) that smoothly deforms the camber over the aft section of the airfoil. A comprehensive rotorcraft aeromechanics analysis was used that modeled the blade elastic motion using one-dimensional finite beam elements combined with multibody dynamics. Aerodynamic forces were calculated with a free-vortex wake model together with lifting line theory for the blade aerodynamics. The open-loop investigation comprised of a parametric study of relevant control parameters that govern the active camber deflection cyclic actuation profile and their effects on rotor performance and hub vibration. It was found that active camber morphing using superimposed once-per-revolution (1P) and 2P control inputs was able to simultaneously reduce rotor power by 4.3% and overall vibratory hub loads by 27%. Additionally, a closed-loop adaptive multicyclic controller was used to identify the potential of this morphing concept for hub vibration reduction using multicyclic active control inputs. Active camber actuation using a sum of four control harmonic inputs, i.e. 1-4P, resulted in a maximum hub vibration reduction of 50%.

*Address all correspondence to this author. Email: sumeet.kumar@tum.de

NOMENCLATURE

A_{mP}	Amplitude of mP active camber actuation harmonic input, deg
c	Blade chord, m
$\boldsymbol{C}$	Gain matrix relating the hub vibration response to the feedback control inputs
C_l	2-D section lift coefficient
C_P	Rotor power coefficient, $P/\pi\rho R^2(\Omega R)^3$
C_H	Drag force coefficient (shaft axis), $H/\pi\rho R^2(\Omega R)^2$
C_T	Rotor thrust coefficient (shaft axis), $T/\pi\rho R^2(\Omega R)^2$
F_X	Non-rotating 4/rev longitudinal hub shear force
F_Y	Non-rotating 4/rev lateral hub shear force
F_Z	Non-rotating 4/rev vertical shear force
M_X	Non-rotating 4/rev hub roll moment
M_x	Steady hub roll moment (shaft axis, right wing up positive), Nm
M_Y	Non-rotating 4/rev hub pitching moment
M_Z	Non-rotating 4/rev hub yaw moment
J	Rotor hub vibration index
J_{obj}	Cost function of the closed-loop multicyclic controller
M	Mach number
N	Number of rotor blades
r	Radial position of the center of the active camber morphing section normalized by the rotor radius
R	Rotor radius, m

s	Spanwise length of the active camber section normalized by rotor radius
$\boldsymbol{T}$	Transfer matrix relating the active control input vector $\boldsymbol{\theta}$ and the hub vibration response vector $\boldsymbol{z}$
mP	m times the rotor rotational frequency
v	Forward flight velocity, m/s
$\boldsymbol{W_z}$,$\boldsymbol{W_\theta}$,$\boldsymbol{W_{\Delta\theta}}$	Weighting matrices for the response, control and control perturbation, respectively
$\boldsymbol{z}$	Response vector containing harmonic Fourier coefficients of hub shear forces and bending moments
α_s	Rotor shaft tilt (negative forward), deg
δ	Active camber deflection, deg
δ_0	Mean active camber deflection, deg
Δ	Denoting change in quantity compared to baseline result
μ	Advance ratio, $v/\Omega R$
ϕ_{mP}	Phase of mP active camber actuation input, deg
Ω	Rotor angular velocity, rad/s
ψ	Rotor azimuth (measured counter-clockwise) , deg
σ	Rotor solidity, $Nc/\pi R$
$\boldsymbol{\theta}$	Input vector containing harmonic Fourier coefficients of active camber deflection

INTRODUCTION

Helicopters generate lift due to the rotary motion of the wings (i.e. the rotor blades), unlike their fixed-wing counterparts. As a result, during forward flight, the oncoming flow velocity experienced by different blade sections varies over the blade span and over the rotor azimuth. The blades need to be pitched with cyclic frequency Ω, i.e. once-per-revolution (1P), to maintain the balance of thrust between the contribution from the advancing side of the rotor disk, where the dynamic pressure is high, and from the retreating side where the dynamic pressure is low. The flexibility of slender rotor blades combined with the unsteady aerodynamic loading, due to varying oncoming flow velocity and blade pitching, results in high dynamic blade loads that are peculiar to rotors in edgewise flight.

Rotors with structurally and aerodynamically identical blades only transmit vibratory loads to the non-rotating hub frame at multiples of the blade passage frequency, i.e. mNP harmonics are transmitted to the hub (where m =1,2,3, etc.) [1]. The non-rotating hub vibration will be referred to as just hub vibration from here on. The $mN-1$P and $mN+1$P harmonics of rotor in-plane forces, i.e. chordwise and centrifugal blade forces, produce the mNP hub shear loads. The $mN-1$P and $mN+1$P harmonics of blade flapping loads produce the mNP hub roll and pitching moments. The mNP out of plane shear forces and rotor yaw moments get directly transmitted to the hub. Therefore, the 3P, 4P and 5P blade loads in the rotating blade frame contribute to the 4P hub vibratory loads of a four-bladed rotor. The 1P and the 2P harmonic components of the blade loads, that generally have a higher magnitude compared to other harmonic components, do not affect the vibration at the rotor hub at all.

The goal of ameliorating vibratory loads within the rotorcraft fuselage to improve comfort of ride and decrease overall maintenance costs by reducing fatigue loads on critical components, has been an active research area. Use of both passive and active vibration reduction methods have been studied. Passive methods refer to using vibration absorbers such as bifilars or pendulum absorbers on the rotor that are tuned to attenuate the response at only certain frequencies [2]. Since rotor vibrations are a consequence of complex rotor aeroelastic effects, investigations have been carried out where the blade structural and geometric properties were optimized such that the resulting hub vibration was minimized [3, 4]. Active vibration control methods refer to installing mechanisms either in the non-rotating frame, for e.g., higher harmonic control via the swashplate, or in the rotating frame, for e.g., individual blade control via pitch-link actuators or through on-blade active mechanisms. These mechanisms are capable of being actuated at multiples of rotor rotation frequencies (i.e. mP) to modify the unsteady aerodynamic loading on the blades.

In the past, several active rotor control concepts have been investigated for performance enhancement and vibration reduction. Generally, the focus has been on up to 2P active control for performance improvement. Active rotor control investigations of different active concepts have demonstrated that any performance improvement using up to 2P active control is largely a result of rotor thrust redistribution from the front and aft sections of the rotor disk to the lateral sides [5–10]. In Ref. [11], it was shown that the underlying physical mechanisms responsible for performance improvement using the active camber morphing rotor, also investigated in the current work, were similar in principle.

The velocity over the rotor azimuth has a mean value equal to the forward flight velocity and a 1P component arising from the rotation of the blades. A 1P active input on the rotor blade changes the section aerodynamic characteristics at a frequency of 1P. Multiplied with the periodic dynamic pressure experienced over every section of the blade, a 1P active control input is capable of affecting shear forces and bending moments on the rotating blade at up to 3P (i.e. $(N-1)$P for a four-bladed rotor), and thereby influence the hub vibration. Similarly, 2P active input also influences vibratory hub loads by influencing blade loading at up to 4P harmonics. Therefore, higher harmonic actuation input to the rotor blade for the purpose of performance improvement, either due to on-blade active control mechanisms or due to individual blade control (IBC) input at the blade-root via pitch link actuators, can affect hub vibration.

Wind-tunnel tests of the full-scale Bo 105 helicopter rotor using 2P IBC via pitch-links reported a significant reduction in vibratory hub loads over a range of phase input during low speed ($\mu = 0.1$) forward flight [6]. However, no vibration reduction

was measured at high-speed forward flight ($\mu = 0.3$). Similar tests using a full-scale UH-60 helicopter rotor at the forward flight transition velocity ($\mu = 0.1$) also resulted in reduced hub vibration using only 2P harmonic IBC control at different phase of control inputs [12]. A later study in Ref. [7] involving high speed forward flight tests with 2P IBC inputs focused only on the corresponding performance gain and the effect on hub vibratory loads was not reported. Ref. [13] presents some limited measurements of vertical hub vibratory shear force based on wind-tunnel tests of a scaled rotor model with trailing-edge flaps (TEFs). The reported measurements showed the potential of partial span TEFs to reduce hub vibration using just 1P or 2P harmonic inputs. Under a Smart-Twisting Active Rotor (STAR) program a 40% Mach-scaled Bo 105 rotor, but with articulated hinges and without any pre-cone, was modified to allow active twist of the blades [14]. A CFD-CSD coupled analysis showed that using only 1P or 2P active twist actuation at $\mu = 0.35$ it was possible to reduce hub vibration. The simultaneous reduction in rotor power was nominal. In Ref. [15], a CFD-CSD coupled analysis of a UH-60 helicopter using trailing-edge deflection also showed that, using only 1P or 2P active control, simultaneous performance improvement and hub vibration reduction was possible.

Woods et al. [16] proposed an active camber morphing concept, called the Fish Bone Active Camber (FishBAC), that is capable of smoothly deforming the camber in the aft section of an airfoil. Based on 2-D wind tunnel tests, the FishBAC mechanism was demonstrated to be aerodynamically more efficient compared to an airfoil with an equivalent size trailing-edge flap due to the more streamlined, continuous profile. Ref. [17] used CFD analysis to quantify the differences between steady aerodynamic coefficients of airfoil profiles with different degrees of camber morphing, introduced by the FishBAC concept. A NACA23012 was used as the baseline airfoil for the analysis. The airfoil tables generated based on this study were then used in a comprehensive rotor aeromechanics analysis to investigate the potential of this morphing concept to improve overall rotor performance [11]. This investigation involved a parametric study of design and control variables, associated with the active camber morphing section, with up to 2P control input. Initial parametric sweep studies showed that a maximum power reduction of 4.4% could be achieved by placing the morphing section from $0.5R$ to $0.9R$ radial span of the blade and using a combined 1P+2P active control input.

In the current study, both open-loop and closed-loop control investigations were carried out to exhibit the potential of the active camber morphing mechanism to reduce hub vibration, while maintaining most of the performance improvements. The open-loop control investigation involved a parametric study of control variables that define the cyclic active camber deflection profile. The focus was on identifying optimal 1P+2P control that led to simultaneous gain in performance and reduction in hub vibration. The closed-loop control investigation involved a deterministic self-tuning multicyclic controller described in Ref. [18]. A sum of four and five control input harmonics, 1-4P and 1-5P, respectively, was used to identify the potential of the camber morphing mechanism to reduce hub vibration only.

METHODOLOGY

The current investigation was based on a comprehensive rotor aeromechanics analysis model of an isolated Bo 105 rotor. The comprehensive analysis code used for the computations was CAMRAD II [19], which comprises a numerical computation of multibody dynamics, rigid and elastic blade motion and aerodynamic forces of a rotor system.

Modeling Framework

The rotor elastic motion was solved based on a harmonic solution method assuming Euler-Bernoulli beam theory for isotropic materials. The blade was discretized by seven elastic beam elements along the span, each with six rigid and seven elastic degrees of freedom. Structural properties of the baseline blade were defined at 41 radial stations along the blade span and integrated over each beam element. A rotor azimuthal step size of 15° was used throughout the study to ensure computational efficiency. The active blade cross section (see Fig. 1) requires reasonable modifications in comparison to the baseline blade due to integration of the active camber mechanism. These modifications result in different blade structural properties. However, both baseline and morphed camber blade cases were computed with the known baseline blade structural properties to isolate the aerodynamic effects of inducing blade camber morphing.

The blade aerodynamic forces were calculated by lifting line theory using airfoil look-up tables. These look-up tables contained the 2D airfoil coefficients (C_l, C_d, C_m) of the blade profile in dependence of angle of attack, Mach number and magnitude of camber deflection, further elaborated in [17]. Each blade was discretized by 28 aerodynamic panels distributed non-uniformly along the blade span. Unsteady aerodynamics were accounted for using the ONERA EDLIN model [20].

The rotor flow field was computed with a free vortex wake method using four trailers along the span. Two trailers were placed at the ends of the blade aerodynamic section ($0.22R$ and $1.00R$) and two trailers at the ends of the active camber section. A Bagai-Leishman vortex model was used to define the transition from a Rankine core vortex model to the potential vortex model used for the far field. The rotor wake was truncated after five rotor revolutions. A full distortion of the rotor trailed and shed vorticity was calculated for three rotor revolutions. The validation of this computational model framework for this rotor was shown in [11].

Based on a previous study regarding rotor performance im-

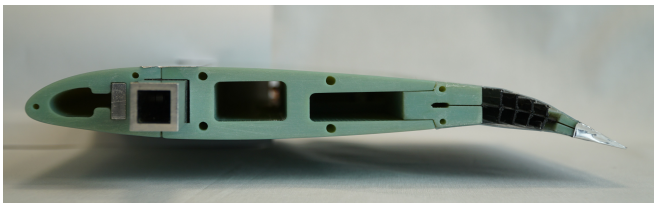

(a) CROSS SECTION OF THE MORPHING SECTION

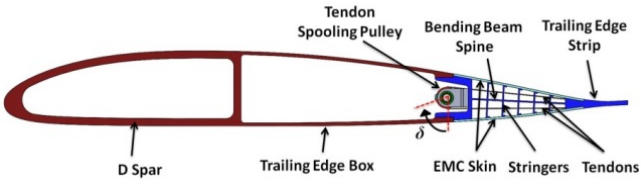

(b) ILLUSTRATION OF THE CROSS SECTION DETAILS

FIGURE 1: CROSS SECTIONAL LAYOUT OF THE FISHBAC ACTIVE CAMBER MORPHING CONCEPT.

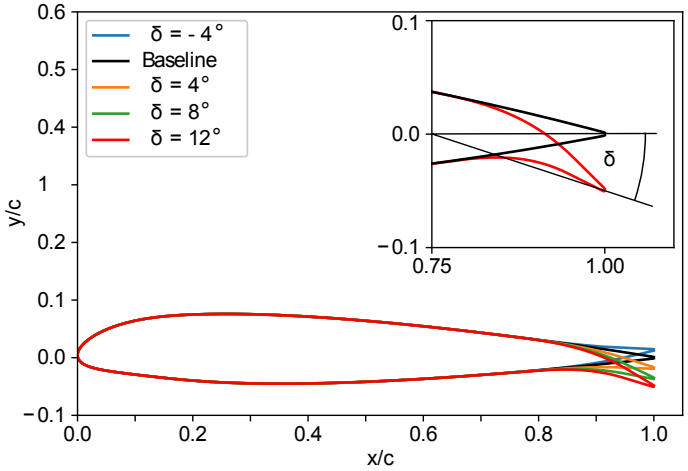

(a) ACTIVE CAMBER PROFILES AND δ DEFINITION

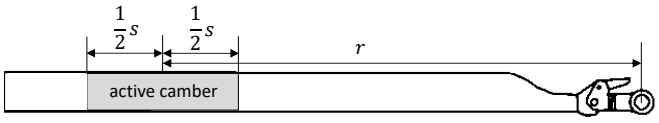

(b) ACTIVE CAMBER DESIGN PARAMETERS

FIGURE 2: GEOMETRIC DEFINITIONS FOR THE ACTIVE CAMBER CONCEPT.

provement with active camber actuation [11], the active camber mechanism was implemented on the blade from $0.5R$ to $0.9R$. Such a configuration proved to be most efficient in terms of rotor performance improvement. The first 75% of the chord were equivalent to the NACA23012 baseline airfoil, and only the aft 25%c were continuously deformed. The camber deflection, described by the symbol δ (see Fig. 2a), was defined as a superposition of harmonic inputs following Eqn. (1). The radial position and the extent of the active section are defined in Fig. 2b.

$$\delta = \delta_0 + \sum_m A_{\mathrm{mP}} \cdot cos(m\psi - \phi_{\mathrm{mP}}) \tag{1}$$

The following trim conditions were used throughout the current investigation: $\alpha_s = -6.0°$, $\mu = 0.3$, $C_T/\sigma = 0.089$, $M_x = 1000$ Nm and $C_H/\sigma = 0.0$. These trim conditions correspond to a fast forward flight state of a Bo 105 during flight test [21].

Open-Loop Investigation

An open-loop investigation was carried out using 1P, 2P and superimposed 1P+2P active control inputs to the morphing camber section installed on the rotor blades. These inputs were predefined and their effect was incorporated within the rotor trim loop so that the same trim state is maintained throughout the investigation. The objective of the open-loop investigation was to identify potential active camber cyclic deflection profiles that resulted in simultaneous reduction in rotor power as well as reduction in hub vibration. The focus was on the range of values of control variables δ_0, $\phi_{1\mathrm{P}}$, $\phi_{2\mathrm{P}}$, $A_{1\mathrm{P}}$, and $A_{2\mathrm{P}}$ in Eqn. (1) that was already identified in Ref. [11] to result in a reduction in rotor power. Within this range, further investigation was targeted towards the identification of cases that also led to hub vibration reduction. The non-dimensional rotor power coefficient C_P was used as a measure of the rotor power, and the non-dimensional hub vibration index J (see Eqn. (2)) was used as a measure of the rotor hub vibration. In Eqn. (2), the quantities F_{X0}, F_{Y0} etc. refer to the corresponding baseline rotor results.

$$J = \sqrt{\left(\frac{F_X}{F_{X0}}\right)^2 + \left(\frac{F_Y}{F_{Y0}}\right)^2 + \left(\frac{F_Z}{F_{Z0}}\right)^2 + \left(\frac{M_X}{M_{X0}}\right)^2 + \left(\frac{M_Y}{M_{Y0}}\right)^2 + \left(\frac{M_Z}{M_{Z0}}\right)^2} \tag{2}$$

Closed-Loop Investigation

In addition to the open-loop active control study with up to 2P harmonics, a deterministic closed-loop controller with feedback was used to investigate the potential of the morphing rotor to reduce only the hub vibratory loads. The controller used in this study is detailed in Ref. [18]. The controller was based on the assumption of a linear, quasi-static frequency domain representation of the rotor system. A linear transfer function $\boldsymbol{T}$ was used to relate the Fourier components of any multi-harmonic control input $\boldsymbol{\theta}$ to those of the resultant hub loads $\boldsymbol{z}$. The assumption was based on experimental measurements that indicated that

higher harmonic control amplitudes required for vibration reduction were of the order of $0.5^\circ - 1.5^\circ$ [2]. It was implemented using Eqn. (3) where $\boldsymbol{z}_k$ is a vector whose elements are the Fourier components of the hub shear forces and the bending moments, and $\boldsymbol{\theta}_k$ is a vector of the Fourier components of the active control cyclic actuation (see Eqn. (4)).

$$\boldsymbol{z}_k = \boldsymbol{z}_{k-1} + \boldsymbol{T}\left(\boldsymbol{\theta}_k - \boldsymbol{\theta}_{k-1}\right) \tag{3}$$

$$\boldsymbol{z}_k = \begin{bmatrix} F_{Xcos} \\ F_{Xsin} \\ \vdots \\ M_{Zcos} \\ M_{Zsin} \end{bmatrix}_k, \boldsymbol{\theta}_k = \begin{bmatrix} \delta_{1cos} \\ \delta_{1sin} \\ \delta_{2cos} \\ \vdots \end{bmatrix}_k \tag{4}$$

The $\boldsymbol{T}$ matrix was identified using element-wise perturbation of the control inputs in $\boldsymbol{\theta}_k$, at every k-th step in the trim iteration loop when the rotor state changed, and the corresponding $\boldsymbol{z}_k$ vectors were obtained. The objective function was given by Eqn. (5) where $\boldsymbol{W_z}, \boldsymbol{W_\theta}, \boldsymbol{W_{\Delta\theta}}$ are weighting matrices with diagonal entries. A performance penalty could be imposed to avoid optimal control vector solutions that exceed practical limits. This is exercised through $\boldsymbol{W_\theta}$ and $\boldsymbol{W_{\Delta\theta}}$ in Eqn. (5).

$$J_{obj} = \boldsymbol{z}_n^T \boldsymbol{W_z} \boldsymbol{z}_n + \boldsymbol{\theta}_n^T \boldsymbol{W_\theta} \boldsymbol{\theta}_n + \boldsymbol{\Delta\theta}_n \boldsymbol{W_{\Delta\theta}} \boldsymbol{\Delta\theta}_n \tag{5}$$

For the current study, no constraints were placed on the rate of change of active control or the magnitude of the control input. Therefore, $\boldsymbol{W_\theta}$ and $\boldsymbol{W_{\Delta\theta}}$ were zero matrices. Additional, $\boldsymbol{W_z}$ had all unit diagonal entries. The controller operated on the principle of identifying $\boldsymbol{\theta}_n$ that minimizes J_{obj}. Substituting Eqn. (3) in Eqn. (5) to identify $\boldsymbol{\theta}_n$ that minimizes J_{obj} (i.e. $\partial J_{obj}/\partial \theta_n = 0$), the iterative updates within the controller are governed by Eqns. (6) and (7). A relaxation factor λ, in the estimation of the gain matrix, was additionally introduced to improve the rate of convergence.

$$\boldsymbol{\Delta\theta}_n = \boldsymbol{C}\boldsymbol{z}_{n-1} \tag{6}$$

$$\boldsymbol{C} = -\lambda \left(\boldsymbol{T}^T \boldsymbol{W_z} \boldsymbol{T}\right)^{-1} \boldsymbol{T}^T \boldsymbol{W_z} \tag{7}$$

Estimation of the $\boldsymbol{T}$ matrix, and the corresponding gain matrix $\boldsymbol{C}$, were carried out within the rotor trim iterative loop whenever the rotor state changed. Based on Eqn. (6), the active control input was iteratively updated until the assumed performance criterion tolerance was met i.e. $\sqrt{J_{obj}}$ <tolerance. The tolerance was progressively lowered until it was no longer possible to satisfy the controller convergence criteria and rotor trim simultaneously.

RESULTS AND DISCUSSION

The primary focus in the current study was on the largest morphing section extending from $0.5R$ to $0.9R$, i.e. [$r = 0.7$, $s = 0.4$] (see Fig. 2b). This morphing section showed the most potential for performance improvement. Additionally, a smaller morphing section [$r = 0.8$, $s = 0.2$] was also part of the superimposed 1P+2P open-loop investigation. The closed-loop investigation used only the [$r = 0.7$, $s = 0.4$] active section.

Figures 3a and 3b show that isolated 1P and 2P harmonic actuation of the morphing camber section has little potential for vibration reduction. A downward mean deflection of $\delta_0 = 1^\circ$ (see Eqn. (1)) was used for the parametric sweeps since a negative δ_0 did not yield any performance gain [11]. The hub vibratory loads increased over the entire range of the input phase. Figures 4a and 4b show the corresponding effect on rotor power. Figure 5 shows the rotor power and hub vibration results obtained based on full-factorial parametric study. The range of values studied were: $\delta_0 = -1^\circ$ to 4°, $A_{1P} = 0^\circ$ to 5.5°, $A_{2P} = 0^\circ$ to 2.5° and ϕ_{1P},ϕ_{2P}=0° to 360°. It is evident that simultaneous reduction in rotor power and in hub vibration is not possible using single harmonic inputs of up to 2P.

Figure 6 shows rotor power results corresponding to the superimposed 1P+2P actuation input study for the two different geometric design configurations considered, namely [$r = 0.7$, $s = 0.4$] and [$r = 0.8$, $s = 0.2$]. Values of the control variables ϕ_{1P}, ϕ_{2P}, A_{1P}, and A_{2P} in Eqn. (1) were chosen such that the resulting performance gain was close to the maximum power reduction that was possible for the respective geometric design configurations. A parametric sweep of varying actuation phasing, ϕ_{2P}, revealed that best performance was possible over a much broader range of ϕ_{2P}, depending on the different combinations of the aforementioned control variables.

An analysis of the vibration indices showed that only specific actuation profiles that led to performance enhancement also resulted in vibration reduction (see Fig. 7). It is worth noting that within the same range of ϕ_{2P} investigated, i.e. 210° to 290° for the [$r = 0.7$, $s = 0.4$] case, the increasing J trend towards higher ϕ_{2P} was similar to the isolated 2P input result shown in Fig. 3b. Unlike shown in Fig. 7a, a distinctive minimum for hub vibration was not obtained for the [$r = 0.8$, $s = 0.2$] geometric design configuration (shown in Fig. 7b), within the scope of the parametric study. Expanding the scope of investigation was not deemed necessary due to the progressive loss of performance gain with further decrease in ϕ_{2P}. For both of the design configurations considered, it is evident that simultaneous reduction in vibration and rotor power is possible using superimposed 1P+2P actuation. Similar trends were observed upon conducting a parameter sweep of ϕ_{1P}, while keeping all the other control variables fixed, and therefore these results have not been reported here.

Figure 8 shows results based on a full-factorial parametric study of control variables within ranges that were found to be promising for performance enhancement. It can be seen

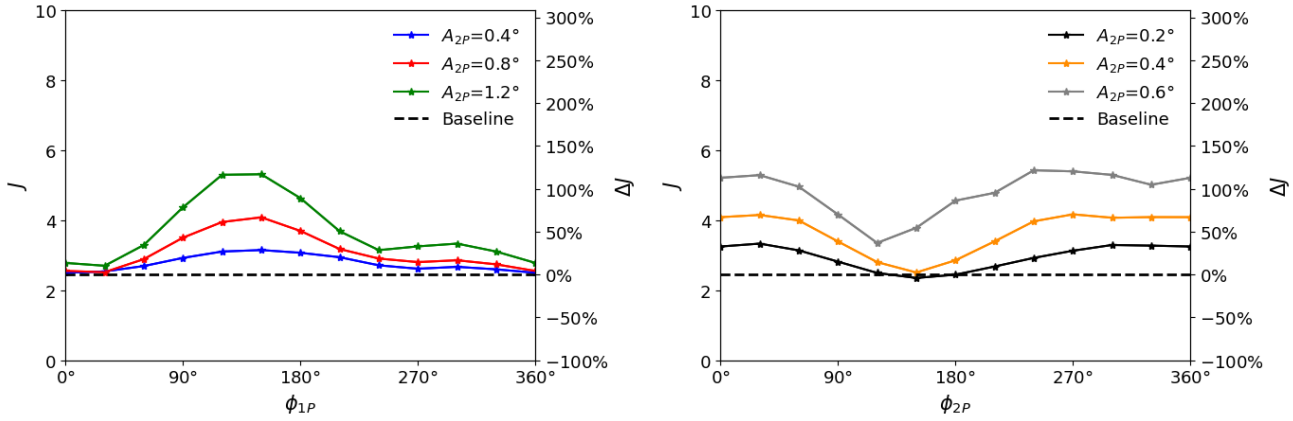

(a) 1P (b) 2P

FIGURE 3: EFFECT OF ISOLATED 1P AND 2P ACTIVE CONTROL INPUT ON ROTOR HUB VIBRATION INDEX J FOR SEVERAL DEFLECTION AMPLITUDES. ($\delta_0 = 1°$)

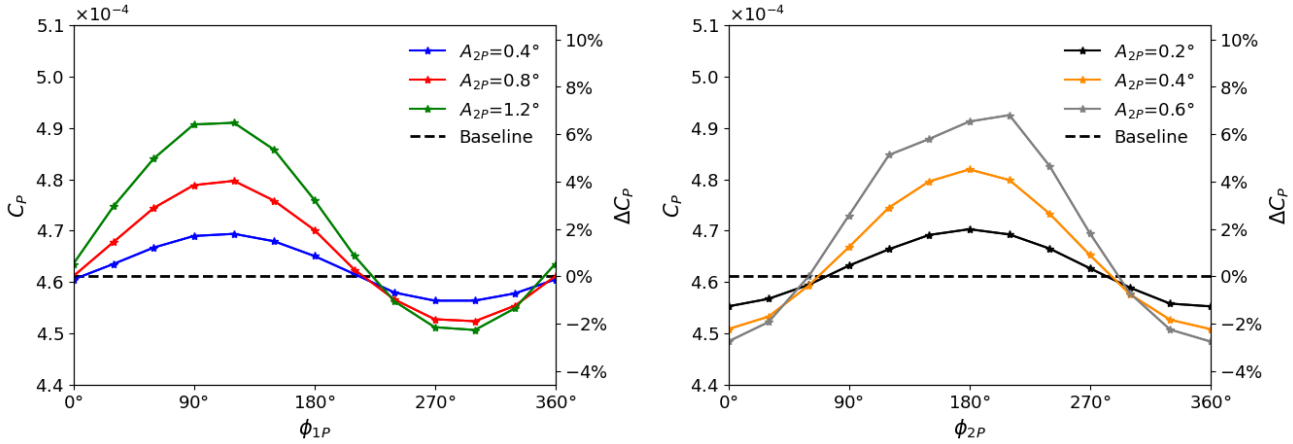

(a) 1P (b) 2P

FIGURE 4: EFFECT OF ISOLATED 1P AND 2P ACTIVE CONTROL INPUT ON ROTOR POWER COEFFICIENT C_P FOR SEVERAL DEFLECTION AMPLITUDES. ($\delta_0 = 1°$)

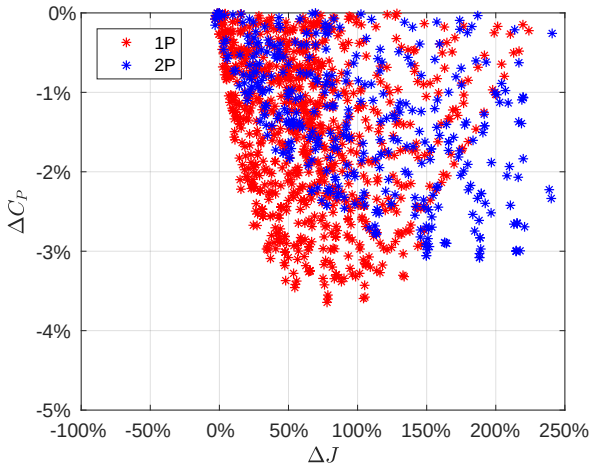

FIGURE 5: ROTOR POWER AND HUB VIBRATION RESULTS BASED ON THE FULL-FACTORIAL PARAMETRIC STUDY OF CONTROL VARIABLES FOR ISOLATED 1P AND 2P INPUT.

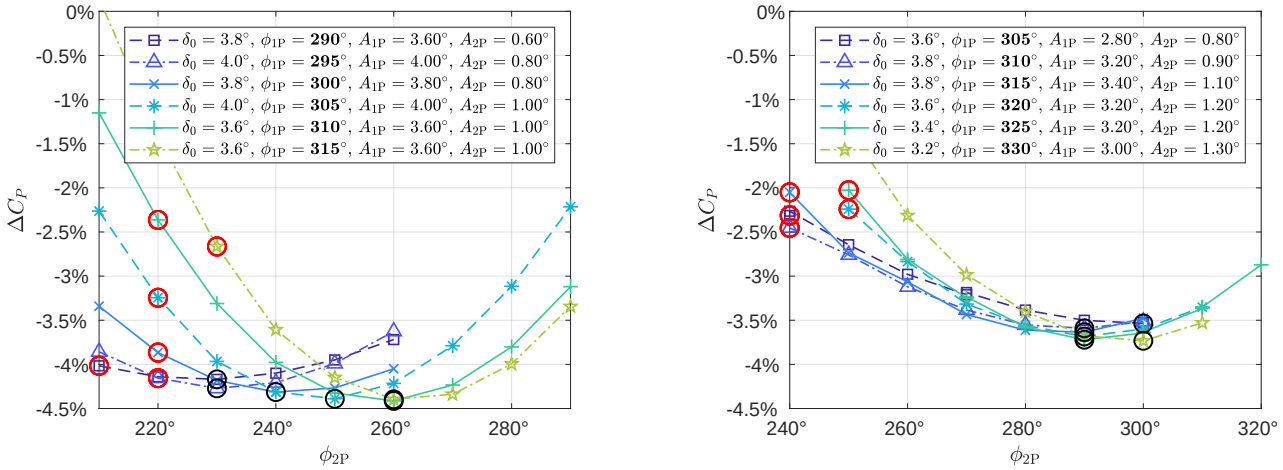

(a) $r = 0.7$, $s = 0.4$ (b) $r = 0.8$, $s = 0.2$

FIGURE 6: EFFECT OF SUPERIMPOSED 1P+2P ACTIVE CAMBER ACTUATION ON ROTOR POWER.

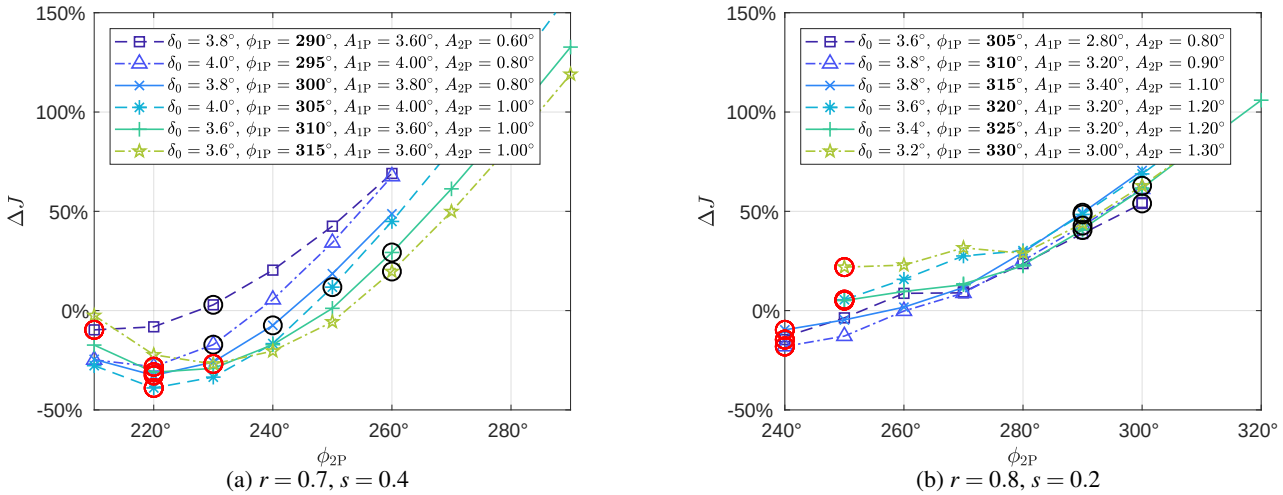

(a) $r = 0.7$, $s = 0.4$ (b) $r = 0.8$, $s = 0.2$

FIGURE 7: EFFECT OF SUPERIMPOSED 1P+2P ACTIVE CAMBER ACTUATION ON HUB VIBRATION.

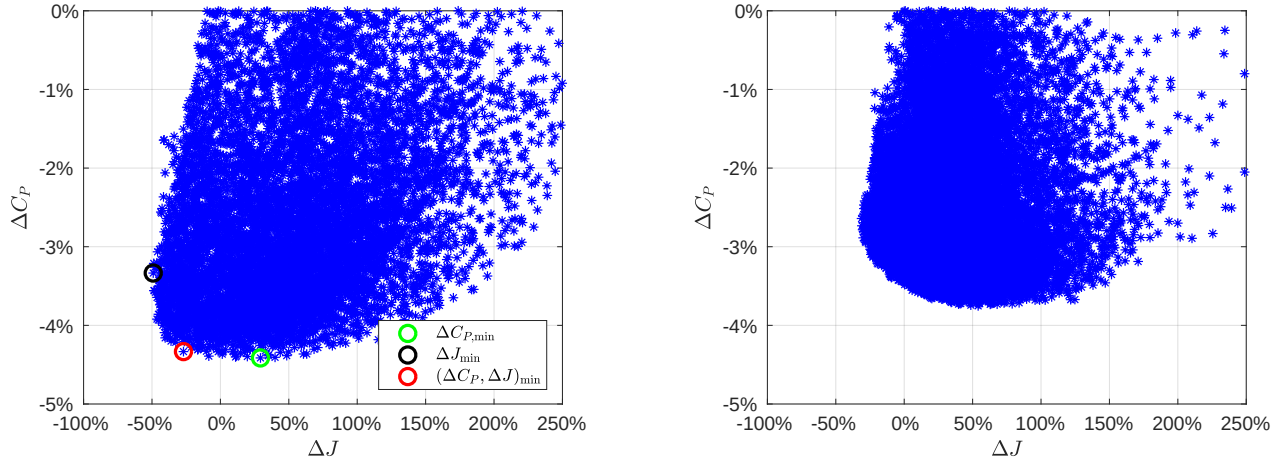

(a) $r = 0.7$, $s = 0.4$ (b) $r = 0.8$, $s = 0.2$

FIGURE 8: ROTOR POWER AND HUB VIBRATION RESULTS BASED ON THE FULL-FACTORIAL PARAMETRIC STUDY OF CONTROL VARIABLES (SUPERIMPOSED 1P+2P STUDY) FOR TWO DIFFERENT SIZES AND RADIAL PLACEMENT OF ACTIVE MORPHING SECTION.

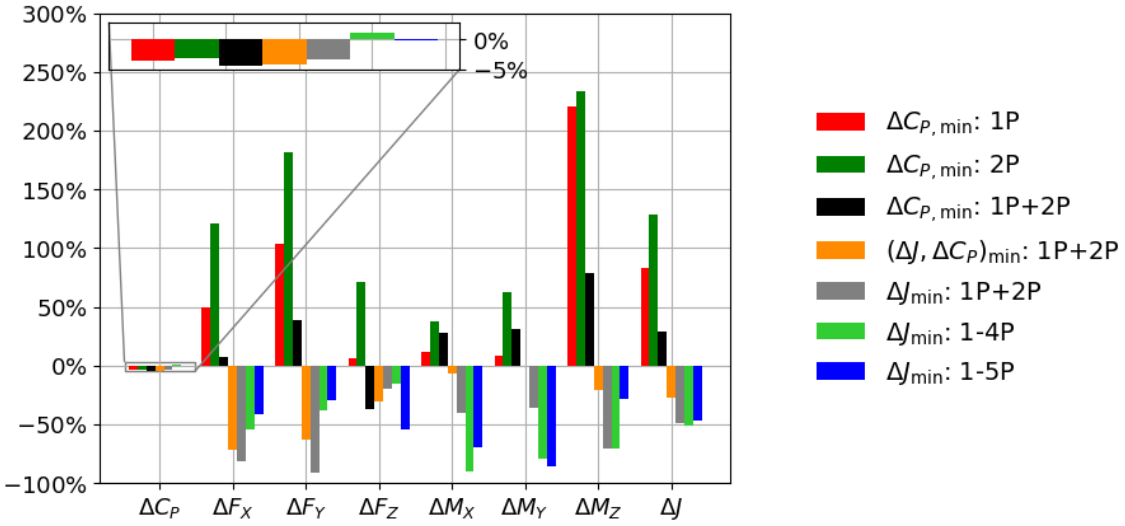

FIGURE 9: ROTOR HUB 4P VIBRATORY LOADS, VIBRATION INDEX AND ROTOR POWER COMPARISON OF OPTIMAL HARMONIC CONTROL INPUTS THAT OPTIMIZE FOR ROTOR POWER (C_P) OR HUB VIBRATION (J) OR BOTH (J, C_P).

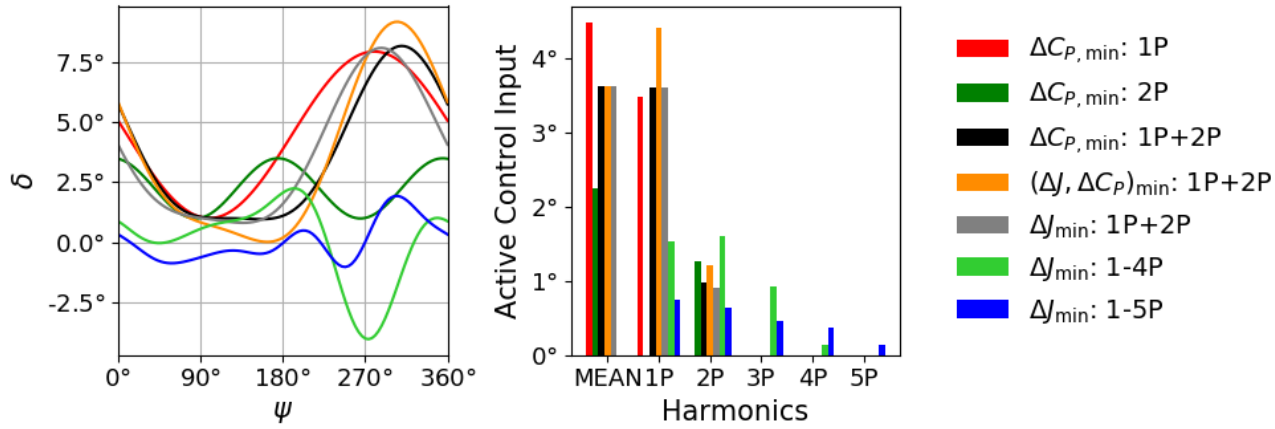

FIGURE 10: ACTIVE CAMBER DEFLECTION PROFILES AND CORRESPONDING HARMONIC COMPONENTS THAT LEAD TO RESULTS SHOWN IN FIG. 9.

in Fig. 8a that with superimposed 1P+2P active control input the best performance case with $\Delta C_P = -4.4\%$ also resulted in an increase in hub vibration by 29% ($\Delta C_{P,\text{min}}$, result circled in green). However, up to 49% reduction in hub vibration was possible by forgoing a nominal amount of performance gain, i.e. $\Delta C_P = -3.3\%$ (ΔJ_{min}, result circled in black). Overall, the active control input that resulted in $\Delta C_P = -4.3\%$ and $\Delta J = -27\%$ was determined to provide the best compromise between performance gain and hub vibration reduction ($(\Delta C_P, \Delta J)_{\text{min}}$, result circled in red). For the $[r = 0.8, s = 0.2]$ configuration, the maximum hub vibration reduction was limited to 31% and the corresponding power reduction was -2.8%.

The closed-loop investigation focused only on the $[r = 0.7, s = 0.4]$ geometric section using 1-4P and 1-5P active control input harmonics. The cost function (see Eqn. 5) comprised of the Fourier coefficients of the 4P hub shear forces and bending moments. The adaptive feedback of the controller was guided by minimization of this cost function (see Eqns. 6 and 7). The mean deflection δ_0 was zero for the closed-loop investigation.

Figures 9 and 10 summarize the results obtained as part of both the open-loop and the closed-loop investigations. Figure 9 shows the rotor power, hub vibratory shear forces and bending moments, and the hub vibration indices for active camber deflections based on different control input harmonics. These active control inputs were targeted towards minimizing rotor power ($\Delta C_{P,\text{min}}$) or minimizing hub vibration (ΔJ_{min}) or simultaneously

achieving both ($(\Delta J, \Delta C_P)_{\min}$). Figure 10 shows the corresponding cyclic deflection profiles and the magnitudes of the contributing individual harmonic inputs. The results for isolated 1P and 2P active control inputs, that minimized C_P, showed an increase in all hub vibratory loads. The results corresponding to the three cases highlighted in Fig. 8a for the superimposed 1P+2P study are also presented. Small differences in the constituent harmonic inputs, governing the superimposed 1P+2P deflection profiles (see Fig. 10), had a greater impact on the hub vibratory loads than the rotor power. Using the closed-loop controller with feedback, it was possible to reduce hub vibration by up to 50% and 47% using a combination of harmonic inputs of 1-4P and 1-5P, respectively. Given that the controller convergence criteria was based on $\sqrt{J_{obj}}$ <tolerance, it is possible that a local minimum was encountered during the closed-loop investigation rather than a global minimum.

SUMMARY AND CONCLUSIONS

A full-scale Bo 105 helicopter rotor with a novel active camber morphing concept was investigated in this study. The objective was to quantify the potential of this active rotor to improve rotor performance and reduce hub vibratory loads. An open-loop investigation with isolated 1P and 2P control input, and superimposed 1P+2P active control inputs was conducted to assess the potential for simultaneous improvement in rotor performance and reduction in hub vibration. Additionally, a closed-loop control investigation with adaptive feedback was also conducted to asses the maximum hub vibration reduction possible using control inputs with sums of four and five input harmonics, i.e. 1-4P and 1-5P, respectively.

Based on the open-loop investigation with isolated 1P and 2P control inputs, it was found that the current active camber morphing concept cannot simultaneously lead to reduced rotor power and reduced hub vibratory loads for the hingeless rotor under investigation. However, it was found that this could be achieved using superimposed 1P+2P active control inputs. The optimal 1P+2P cyclic active camber deflection that gave best rotor performance was identified as a non-harmonic curve with a small positive, near-constant deflection on the advancing side of the rotor disk and a large positive harmonic deflection on the retreating side. Such cyclic actuation profiles for 1P+2P input were obtained for different combinations of amplitude and phasing of the individual 1P and 2P harmonic components which affected rotor hub vibration significantly. As a result, it was possible to identify superimposed 1P+2P actuation profiles that led to the following sets of results compared to the baseline rotor: $\Delta C_P = -4.4\%$, $\Delta J = 29\%$; $\Delta C_P = -4.3\%$, $\Delta J = -27\%$ and $\Delta C_P = -3.3\%$, $\Delta J = -49\%$. Increasing the number of constituent harmonics to the active control input and using a closed-loop controller with adaptive feedback did not yield significant additional reduction in hub vibration over what was achieved using the superimposed 1P+2P actuation.

ACKNOWLEDGMENT

This project has received funding from the European Union's Horizon 2020 research and innovation program under grant agreement No. 723491.

REFERENCES

[1] Bramwell, A. R. S., Balmford, D., and Done, G., 2001. *Bramwell's Helicopter Dynamics*. Butterworth Heinemann, ch. 8.

[2] Johnson, W., 2013. *Rotorcraft Aeromechanics*. Cambridge University Press, ch. 18.

[3] Glaz, B., Friedmann, P. P., and Liu, L., 2008. "Surrogate based optimization of helicopter rotor blades for vibration reduction in forward flight". *Structural and Multidisciplinary Optimization,* ***35***(4), pp. 341–363.

[4] Ganguli, R., 2002. "Optimum design of a low vibration helicopter rotor using aeroelastic analysis and response surface approximation". *Journal of Sound and Vibration,* ***258***(2), pp. 327–344.

[5] Celi, R., and Cheng, R. P., 2005. "Optimum two-per-revolution inputs for improved rotor performance". *Journal of Aircraft,* ***42***(6), pp. 1409–1417.

[6] Jacklin, S. A., Blass, A., Swanson, S. M., and Teves, D., 1995. "Second test of a helicopter individual blade control system in the NASA ames 40- by 80-foot wind tunnel". In American Helicopter Society 2nd International Aeromechanics Specialists Conference, Bridgeport, CT.

[7] Norman, T. R., Theodore, C., Shinoda, P., Fuerst, D., Arnold, U. T., Makinen, S., Lorber, P., and ONeill, J., 2009. "Full-scale wind tunnel test of a UH-60 individual blade control system for performance improvement and vibration, loads, and noise control". In American Helicopter Society 65th Annual Forum.

[8] Jain, R., Yeo, H., and Chopra, I., 2010. "Computational fluid dynamics—computational structural dynamics analysis of active control of helicopter rotor for performance improvement". *Journal of the American Helicopter Society,* ***55***(4).

[9] Yeo, H., 2008. "Assessment of active controls for rotor performance enhancement". *Journal of the American Helicopter Society,* ***53***(2), pp. 152–163.

[10] Ravichandran, K., Chopra, I., Wake, B. E., and Hein, B., 2013. "Trailing-edge flaps for rotor performance enhancement and vibration reduction". *Journal of the American Helicopter Society,* ***58***(2), April.

[11] Komp, D., Kumar, S., Abdelmoula, A., Hajek, M., and Rauleder, J., 2019. "Investigation of active rotor design

and control for performance improvement". In American Helicopter Society 75th Annual Forum.
[12] Jacklin, S. A., Haber, A., de Simone, G., Norman, T. R., Kitaplioglu, C., and Shinoda, P., 2002. "Full-scale wind tunnel test of an individual blade control system for a UH-60 helicopter". In American Helicopter Society 58th Annual Forum.
[13] Crozier, P., Leconte, P., Delrieux, Y., Gimonet, B., Le Pape, A., and Mercier de Rochettes, H., 2006. "Wind-tunnel tests of a helicopter rotor with active flaps". In 32nd European Rotorcraft Forum.
[14] Lim, J. W., Boyd Jr, D. D., Hoffman, F., van der Wall, B. G., Kim, D.-H., Jung, S. N., You, Y. H., Tanabe, Y., Bailly, J., Lienard, C., and Delrieux, Y., 2014. "Aeromechanical evaluation of smart-twisting active rotor". In 40th European Rotorcraft Forum.
[15] Jain, R., Yeo, H., and Chopra, I., 2010. "Examination of rotor loads due to on-blade active controls for performance enhancement". *Journal of Aircraft,* ***47***(6), pp. 2049–2066.
[16] Woods, B. K., Bilgen, O., and Friswell, M. I., 2014. "Wind tunnel testing of the fish bone active camber morphing concept". *Journal of Intelligent Material Systems and Structures,* ***25***(7), pp. 772–785.
[17] Abdelmoula, A., and Rauleder, J., 2019. "Aerodynamic performance of morphed camber rotor airfoils". In AIAA Scitech Forum.
[18] Johnson, W., 1982. Self-tuning regulators for multicyclic control of helicopter vibration. NASA TP 1996, March.
[19] Johnson, W., 1994. "Technology drivers in the development of CAMRAD II". In American Helicopter Society Aeromechanics Specialists Conference.
[20] Johnson, W., 1998. "Rotorcraft dynamics models for a comprehensive analysis". In 54th Annual Forum of the American Helicopter Society, Washington, DC.
[21] Langer, H. J., and Tränapp, N., 1993. BO 105 flight test data for a wind tunnel test program. DLR IB 111-93/58.